AD-A194 477 THE GRADIENT METHOD FOR INTERFACE TRACKING(U) NAVAL 1/1
RESEARCH LAB WASHINGTON DC K J LASKEY ET AL 31 MAY 88
NRL-MR-6183

UNCLASSIFIED F/G 17/11 NL

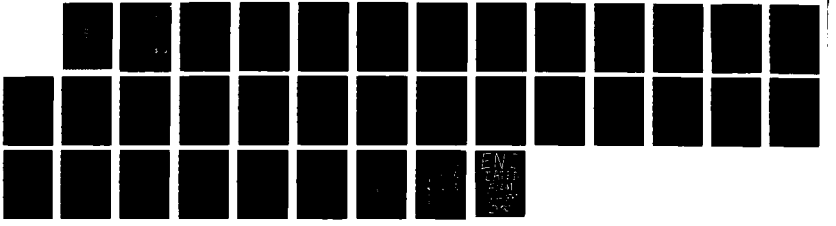

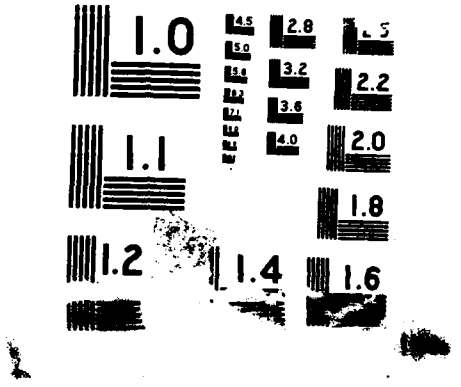
1.0
1.1
1.2
1.4
1.6
1.8
2.0
2.2
2.8
3.2
3.6
4.0
4.5
5.0

NRL Memorandum Report 6183

The Gradient Method for Interface Tracking

K. J. LASKEY,* E. S. ORAN AND J. P. BORIS

**Carnegie-Mellon University, Pittsburgh, PA 15213*
Berkeley Research Associates, Springfield, VA 22150

Center for Reactive Flow and Dynamical Systems
Laboratory for Computational Physics and Fluid Dynamics

May 31, 1988

6a. NAME OF PERFORMING ORGANIZATION	6b. OFFICE SYMBOL (If applicable)	7a. NAME OF MONITORING ORGANIZATION
Naval Research Laboratory	Code 4410	
6c. ADDRESS (City, State, and ZIP Code)		**7b. ADDRESS (City, State, and ZIP Code)**
Washington, DC 20375-5000		
8a. NAME OF FUNDING / SPONSORING ORGANIZATION	**8b. OFFICE SYMBOL (If applicable)**	**9. PROCUREMENT INSTRUMENT IDENTIFICATION NUMBER**
Office of Naval Research		
8c. ADDRESS (City, State, and ZIP Code)		**10. SOURCE OF FUNDING NUMBERS**
Washington, DC	PROGRAM ELEMENT NO. ONR	PROJECT NO. ONR
	TASK NO.	WORK UNIT ACCESSION

11. TITLE (Include Security Classification)

The Gradient Method For Interface Tracking

12. PERSONAL AUTHOR(S)

Laskey,* K.J., Oran, E.S. and Boris, J.P.

13a. TYPE OF REPORT	13b. TIME COVERED	14. DATE OF REPORT (Year, Month, Day)	15. PAGE COUNT
Interim	FROM 10/85 TO present	1988 May 31	35

16. SUPPLEMENTARY NOTATION

*Carnegie-Mellon University, Pittsburgh, PA 15213
Berkeley Research Associates, Springfield, VA 22150

17. COSATI CODES			18. SUBJECT TERMS (Continue on reverse if necessary and identify by block number)
FIELD	GROUP	SUB-GROUP	
			Interface tracking Reacting flows

CONTENTS

THE GRADIENT METHOD FOR INTERFACE TRACKING

Introduction

Interface tracking methods are used in numerical calculations to represent an internal physical boundary as a discontinuity that has important properties distinct from the medium on either side. To approximate the interface as a discontinity, the physical boundary must be thin compared to the domain of interest and the importance of the internal structure of the boundary must be limited to the global effects which the interface method attempts to resolve and simulate. There are several groups of interface methods: surface tracking methods [1,2], which keep track of distinct points on the interface, volume tracking methods [3,4,5], which reconstruct the interface on the basis of a marker quantity assigned to each computational cell, and moving grid methods [6,7,8], which alter the computational grid to keep the interface on cell boundaries. In general, all of these methods break the interface modeling process into three steps: 1) defining the location of the interface, 2) determining the movement of the interface, and 3) incorporating the relevant effects of the physical boundary. Useful summaries of interface tracking are found in the reviews by Hyman [9] and Laskey, et al. [10] and the introductory material by Hirt and Nichols [5].

This paper introduces the gradient method, a new interface method for the subset of interface problems where material on one side of the boundary is converted into the material on the other. The gradient method differs fundamentally from the methods previously mentioned in that it is not necessary to define the location or movement of the interface. Rather, the effects of interface propagation are determined from two characteristics distinct to the physical system. First, large gradients are present as a result of material conversion at the physical interface, and the magnitudes of these gradients are used to identify the computational cells containing the reaction front. Second, the interface propagates at a defined speed in a direction normal to itself. This speed is a global quantity that results from the combined effects of heat transfer, diffusion, chemistry, and other processes relevant to the particular problem. The relatively localized large gradients are combined with the propagation speed to determine the amount of material conversion and thus simulate the movement of the interface. The effects of the interface movement are incorporated without the need to resolve the interface beyond the accuracy inherent in the numerical convection algorithms. Below we show how the method is applied to a problem with propagating chemical reaction fronts.

Manuscript approved December 3, 1987.

The Gradient Method

Consider a system containing a mixture of gases, A and B, which can react to form a product species, C,

$$A + B \rightarrow C \,. \tag{1}$$

Reactions can occur in one or several regions in the system. The boundaries of these reacting regions are reaction fronts with large gradients in species concentrations. In the description that follows, we choose the number density of product C, denoted c, as an indicator of the reaction fronts. Later we consider other possible choices for the indicator variable.

The existence of a reaction front does not directly enter into the governing equations for conservation of mass and momentum. For exothermic reactions, a source term appears in the energy conservation equation, but this source term is a function of reaction rate and ultimately the concentration of the constituent species. Since the product number density has been chosen as the indicator variable, the conservation equation of most interest is that for c. An Eulerian representation for the evolution of the product number density is

$$\frac{\partial c}{\partial t} + \nabla \cdot c\vec{V} = w_c \,, \tag{2}$$

where $\vec{V}$ is the velocity vector of the flow field and w_c is the production term due to the propagating reaction front. The left hand side of Eq. (2) can be solved by any method for solving continuity equations, and the production term is added to the convection solution by timestep splitting methods. The gradient method is used to evaluate w_c. For simplicity, other effects, such as molecular diffusion, have been omitted from Eq. (2), but these may also be included using timestep splitting.

Consider a long enclosure of length L and constant cross section S through which a reaction front is propagating. The reactant and product number densities of the enclosed volume vary with time. As the reaction front propagates along the enclosure, the change in product number density, Δc, is given by

$$\Delta c = \frac{(c_2 - c_1)\, lS}{LS} \,, \tag{3}$$

where c_1 and c_2 are the local product number densities upstream and downstream, respectively, of the reaction front and l is the distance the reaction front has moved along the enclosure during a given period of time. Eq. (3) is valid even if only a portion of the enclosure is considered, as long as that portion contains the reaction front. However, L would then be defined as the length of the portion of the enclosure under consideration. Taking the limit as the length L gets vanishingly small gives

$$\Delta c = |\nabla c|\, l \,, \tag{4}$$

where $|\nabla c|$ is the magnitude of the gradient of the product number density across the reaction front. The distance l is measured normal to the reaction front, which is the same direction as that of the gradient. If the speed of the front is the local burning velocity, then l may be approximated by

$$l = V_b \Delta t \,, \tag{5}$$

where V_b is the local burning velocity and Δt is the time interval. The amount of product formed locally in time Δt as the reaction front moves is

$$\int_t^{t+\Delta t} w_c \, dt = \Delta c = V_b \Delta t \, |\nabla c| \,. \tag{6}$$

The integral of the gradient through the reaction front is fixed by the upstream and downstream values of c and not by the purely numerical details of the gradient resolution. Thus, the integrated amount of product formed is the same as that produced by the propagation of the physical interface. For many reactions characterized by Eq. (1) the burning velocities are available in the literature for various concentrations, temperatures, and pressures. In a numerical simulation, the time interval is the numerical timestep, which is determined by stability criteria of the numerical method or other properties of the coupled system of reactive flow equations.

Calculation of $|\nabla c|$

Let us denote the cell centers of a two-dimensional computational grid as (i,j), where $i = 1,\ldots,n_x$ and $j = 1,\ldots,n_y$, and n_x and n_y are the number of cells in the x and y directions, respectively. Species number densities are defined at these cell centers. A central-difference approximation to a numerical derivative on this grid is second-order accurate if the function in question varies smoothly over the three cells involved. A one-sided difference is only first-order accurate, but the number of cells over which c must vary smoothly is reduced from three cells to two. In the problem of a thin reaction front, we have found that a one-sided difference gives a better approximation to the derivative because the largest change in c usually occurs over only two cells. In the gradient method, both the left and right hand one-sided differences are evaluated, and the value chosen for the x-direction derivative g_x is the one with the largest absolute value. The same procedure is used to determine the y-direction derivative, g_y. This process is summarized:

$$g_{x1}(i,j) = \frac{c_{i+1,j} - c_{i,j}}{x_{i+1} - x_i} \quad , \qquad g_{x2}(i,j) = \frac{c_{i,j} - c_{i-1,j}}{x_{i,j} - x_{i-1}} \tag{7a,b}$$

$$g_{y1}(i,j) = \frac{c_{i,j+1} - c_{i,j}}{y_{j+1} - y_j} \quad , \qquad g_{y2}(i,j) = \frac{c_{i,j} - c_{i,j-1}}{y_j - y_{j-1}} \tag{7c,d}$$

$$g_x(i,j) = \begin{cases} g_{x1} & \\ & \text{if} \\ g_{x2} & \end{cases} \begin{matrix} |g_{x1}| > |g_{x2}| \\ \\ |g_{x2}| > |g_{x1}| \end{matrix} \tag{8a}$$

$$g_y(i,j) = \begin{cases} g_{y1} & \\ & \text{if} \\ g_{y2} & \end{cases} \begin{matrix} |g_{y1}| > |g_{y2}| \\ \\ |g_{y2}| > |g_{y1}| \end{matrix} \tag{8b}$$

Note, x_i and y_j are the x and y locations of the center of cell (i,j) , and g_{x1}, g_{x2}, g_{y1}, and g_{y2} are the one-sided derivatives from which g_x and g_y are chosen. The gradient magnitude $|\nabla c|$ is the magnitude of the vector sum of g_x and g_y,

$$|\nabla c| = \left[g_x^2 + g_y^2\right]^{1/2} \tag{9}$$

Modifications to $|\nabla c|$

The value of $|\nabla c|$ is nonzero whenever the values of c in adjacent cells are not identical. But it is possible for this quantity to be nonzero yet unrelated to the presence of a reaction front, for example, in a compression or rarefaction region. Because this model assumes that the largest gradients are connected with reactions, the problem of unrelated gradients is avoided by defining a minimum gradient for reaction and ignoring any gradient below this critical value. This limit prevents the propagation of the reaction front due to numerical diffusion and restricts the thickness of the reaction front to less than two cells. Without this limit, the reaction front is distributed across too wide a region and the effective burning velocity is too low.

The limiting value of $|\nabla c|$, denoted $|\nabla c|_{crit,1}$, is expressed in the form

$$|\nabla c|_{crit,1}(i,j) = C_1 \, \frac{c_{max}(i,j)}{l_1(i,j)} \, , \tag{10}$$

where C_1 is a constant discussed below and $l_1(i,j)$ is a characteristic length. The quantity $c_{max}(i,j)$ is the maximum possible product number density in cell (i,j), and is calculated as

$$c_{max}(i,j) = c_{i,j} + N_c \min\left[\frac{f_{i,j}}{N_f}, \frac{o_{i,j}}{N_o}\right] \, , \tag{11}$$

where $f_{i,j}$ and $o_{i,j}$ are the fuel and oxidant number densities, respectively, N_f and N_o are the number of fuel and oxidant molecules consumed per reaction, and N_c is the number of product

molecules produced per reaction. The reactants A and B in Eq. (1) are now associated with the fuel and oxidizer.

The characteristic length l_1 is a measure of the distance over which the product number density goes from 0 to c_{max} when a reaction front is present in cell (i,j) and its neighbors. The value of l_1 is defined as the weighted average of the distance between the center of cell (i,j) and the centers of the adjacent cells that contribute most to the value of $|\nabla c|$,

$$\begin{aligned} l_1(i,j) = \{ \; & \max[(|g_{x1}| - |g_{x2}|), 0] * (x_{i+1} - x_i) \\ & + \max[(|g_{x2}| - |g_{x1}|), 0] * (x_i - x_{i-1}) \\ & + \max[(|g_{y1}| - |g_{y2}|), 0] * (y_{j+1} - y_j) \\ & + \max[(|g_{y2}| - |g_{y1}|), 0] * (y_j - y_{j-1}) \; \} \; / \; \{ \; \max[(|g_{x1}| - |g_{x2}|), 0] \\ & \qquad + \max[(|g_{x2}| - |g_{x1}|), 0] \\ & \qquad + \max[(|g_{y1}| - |g_{y2}|), 0] \\ & \qquad + \max[(|g_{y2}| - |g_{y1}|), 0] \; \}. \end{aligned} \tag{12}$$

Note that the denominator in Eq. (12) can alternately be expressed as $\{||g_{x1}|-|g_{x2}|| + ||g_{y1}|-|g_{y2}||\}$. The weighting factors in Eq. (12), the differences between the one-sided derivatives, are constructed so that only the spacings between cell centers of cells containing the reaction front are used to calculate l_1. These cells are identified as having the larger of the magnitudes of g_{x1} and g_{x2} and the larger of the magnitudes of g_{y1} and g_{y2}. Using the difference between magnitudes for the weighting factor serves two purposes. First, the difference filters out any small uniform gradient present throughout the flow. Second, the difference puts most of the weight on the direction in which the gradient is changing fastest. Empirically this results in a more accurate reproduction of the input burning velocity.

The second case in which $|\nabla c|$ must be modified is for cells in which reactions must occur regardless of the calculated magnitude of the gradient. For example, consider Figure 1. If cell $(i-1, j-1)$ is *highly reacted*, a term which is quantified below, then cell (i,j) should react. Cells $(i-1,j)$ and $(i,j-1)$ react because the large amount of product in cell $(i-1,j-1)$ leads to values of $|\nabla c|$ greater than $|\nabla c|_{crit,1}$ in these three cells. But the amounts of product in cells $(i-1,j)$ and $(i,j-1)$ are not sufficient to produce a value of $|\nabla c|$ greater than $|\nabla c|_{crit,1}$ in cell (i,j). Physically, though, the reaction should proceed in the corner of cell (i,j).

Another case in which a cell should react due to proximity to a highly reacted cell is when two reaction fronts are merging. Assume in Figure 2 that cell (i,j) has been reacting due to the

gradient from either of its neighbors. As the reaction proceeds, the value of $c_{i,j}$ increases until the difference between it and its neighbors is not sufficient to produce a value of $|\nabla c|$ greater than $|\nabla c|_{crit,1}$. This cell should continue to react, though, so that the reaction fronts can merge.

It is for situations such as those above that the term *highly reacted* and a second critical gradient magnitude are defined. This second critical value, $|\nabla c|_{crit,2}$, represents a second minimum magnitude of the gradient for cells that are near highly reacted cells. The measure of the degree of reaction in a cell is $F_{i,j}$, the fraction of reaction completed,

$$F_{i,j} = \frac{c_{i,j}}{c_{max}(i,j)} . \tag{13}$$

The maximum value of F for the eight cells neighboring cell (i,j) is $F_{max}(i,j)$. If $F_{max}(i,j)$ exceeds a certain value, F_{crit}, the cell (i,j) is said to be neighboring a highly reacted cell and the magnitude of the gradient associated with cell (i,j) should not be less than $|\nabla c|_{crit,2}$. The value of F_{crit} should not be less than C_1 or else all cells would react before $|\nabla c|$ exceeds $|\nabla c|_{crit,1}$. The value of $|\nabla c|_{crit,2}$ is defined as

$$|\nabla c|_{crit,2}(i,j) = C_2 \, \frac{c_{max}(i,j)}{l_2(i,j)} , \tag{14}$$

where C_2 is a constant and l_2 is a characteristic length. The length l_2 is similar to l_1 except that the weighting factor here is the amount that F for a neighbor cell exceeds the value F_{crit}. This change in weighting factor is because $|\nabla c|_{crit,1}$ is looking for high gradients to indicate reaction, but $|\nabla c|_{crit,2}$ is responding to highly reacted cells.

The characteristic length l_2 depends on whether the highly reacted cell is adjacent to a side of cell (i,j) or on a diagonal. For the adjacent cells,

$$\begin{aligned} l_{2,adj}(i,j) = \{ \; & \max[(F_{i+1,j} - F_{crit}),0] * (x_{i+1} - x_i) \\ & + \max[(F_{i-1,j} - F_{crit}),0] * (x_i - x_{i-1}) \\ & + \max[(F_{i,j+1} - F_{crit}),0] * (y_{j+1} - y_j) \\ & + \max[(F_{i,j-1} - F_{crit}),0] * (y_j - y_{j-1}) \; \} \; / \; \{ \; \max[(F_{i+1,j} - F_{crit}),0] \\ & \qquad + \max[(F_{i-1,j} - F_{crit}),0] \\ & \qquad + \max[(F_{i,j+1} - F_{crit}),0] \\ & \qquad + \max[(F_{i,j-1} - F_{crit}),0] \; \} \end{aligned} \tag{15}$$

and

$$F_{max,adj} = \max(F_{i+1,j}, F_{i-1,j}, F_{i,j+1}, F_{i,j-1}) . \tag{16}$$

Here a characteristic length $l_{2,adj}$ corresponds to the maximum F value of the adjacent cells. A similar calculation relates a characteristic length $l_{2,diag}$ and a corresponding maximum F to the diagonal cells.

$$\begin{aligned} l_{2,diag}(i,j) = \{ & \max[(F_{i-1,j-1} - F_{crit}),0] * ds_{i-1,j-1} \\ & + \max[(F_{i+1,j+1} - F_{crit}),0] * ds_{i,j} \\ & + \max[(F_{i+1,j-1} - F_{crit}),0] * ds_{i,j-1} \\ & + \max[(F_{i-1,j+1} - F_{crit}),0] * ds_{i-1,j} \quad \} \, / \\ & \{ \max[(F_{i-1,j-1} - F_{crit}),0] \\ & + \max[(F_{i+1,j+1} - F_{crit}),0] \\ & + \max[(F_{i+1,j-1} - F_{crit}),0] \\ & + \max[(F_{i-1,j+1} - F_{crit}),0] \, \} \end{aligned} \tag{17}$$

and

$$F_{max,diag} = \max(F_{i-1,j-1}, F_{i-1,j+1}, F_{i+1,j-1}, F_{i+1,j+1}) . \tag{18}$$

Here

$$\begin{aligned} ds_{i,j} &= \left[(x_{i+1} - x_i)^2 + (y_{j+1} - y_j)^2\right]^{1/2} \\ &= \text{distance between centers of diagonal neighbors.} \end{aligned} \tag{19}$$

The characteristic length l_2 is either $l_{2,adj}$ or $l_{2,diag}$, depending on whether $F_{max,adj}$ or $F_{max,diag}$ exceeds the value F_{crit}. If both $F_{max,adj}$ and $F_{max,diag}$ exceed F_{crit}, then $l_2(i,j)$ is set to $l_{2,adj}$ because an adjacent cell will have greater influence on its neighbor than a diagonal cell,

$$l_2(i,j) = \begin{cases} l_{2,adj}(i,j) & \text{if } F_{max,adj} > F_{crit} \\ l_{2,diag}(i,j) & \text{if } F_{max,diag} > F_{crit} \text{ and } F_{max,adj} < F_{crit} \end{cases} \tag{20}$$

and

$$F_{max}(i,j) = \max(F_{max,adj}, F_{max,diag}, F_{i,j}) . \tag{21}$$

The discontinuity of Eq. (21) when $F_{max,adj} = F_{max,diag}$ is not important because this condition does not arise in practice. Also, tests show that, except during early stages of a calculation, $l_2 = l_{2,adj}$ whenever $|\nabla c|_{crit,2}$ is used. Finally, if cell (i,j) is highly reacted but all of its neighbors

are not, then the resulting values from Eqs. (15) and (17) are zero. To insure that Eq. (14) yields a usable value, $l_2(i,j)$ is restricted to a value at least as large as the smallest spacing to a neighbor cell,

$$l_2(i,j) = \max\{l_2 \text{ from eq. (20)}, \min[(x_{i+1} - x_i), (x_i - x_{i-1}), (y_{j+1} - y_j), (y_j - y_{j-1})]\}. \quad (22)$$

Modification for nonuniform temperature field

The propagation of an unconfined flame front is approximately a constant pressure process, but the release of energy introduces large temperature gradients at the front. If the process is to remain isobaric, the temperature change must be reflected in a proportional change in species densities. This process occurs in addition to changes in species density due to chemical reactions.

The present model assumes that large differences in the product number density are the result of chemical reactions and the amount of reaction is proportional to the difference in product number densities in adjacent cells. To avoid having density differences reflecting temperature differences rather than reactions, all calculations are done using number densities scaled to an arbitrary reference temperature, T_{ref}. This scaling is done assuming that all species obey the ideal gas law. Thus, the scaled number density, $c^r_{i,j}$, is given by

$$c^r_{i,j} = c_{i,j} \frac{T_{i,j}}{T_{ref}} . \quad (23)$$

The final value of $|\nabla c|_{i,j}$ is scaled back to the local cell conditions by multiplying by the factor $T_{ref}/T_{i,j}$. It may be possible to avoid this modification if the model is formulated in terms of gradients of mole fraction rather than gradients of number density.

Summary of the calculation of $|\nabla c|$

The calculation of $|\nabla c|$ follows the following steps:

1. Scale the product number densities to the reference temperature.
2. Calculate $|\nabla c|$.
   a. Calculate the sample gradients in the x-direction, $g_{x1}(i,j)$ and $g_{x2}(i,j)$.
   b. Set the x-direction gradient for a cell, $g_x(i,j)$, equal to the sample x-direction gradient with the largest absolute value.
   c. Calculate the sample gradients in the y-direction, $g_{y1}(i,j)$ and $g_{y2}(i,j)$.

d. Set the y-direction gradient for a cell, $g_y(i,j)$, equal to the sample y-direction gradient with the largest absolute value.

e. Calculate the magnitude of the gradient, $|\nabla c|$, equal to the vector sum of its components.

3. Determine the minimum gradient magnitude for reaction, $|\nabla c|_{crit,1}$.
   a. Calculate maximum possible product number density in a cell, $c_{max}(i,j)$.
   b. Calculate the characteristic length l_1.
   c. Calculate the value of $|\nabla c|_{crit,1}(i,j)$.
4. Determine the maximum value of the fraction of reaction completed, $F_{max}(i,j)$ for each cell.
   a. Calculate the fraction of reaction completed for each cell, $F_{i,j}$.
   b. Determine $F_{max,adj}(i,j)$, the maximum value of F for cells adjacent to cell (i,j).
   c. Determine $F_{max,diag}(i,j)$, the maximum value of F for cells on the diagonal of cell (i,j).
   d. Assign the largest of $F_{max,adj}(i,j)$, $F_{max,diag}(i,j)$, and $F_{i,j}$ to $F_{max}(i,j)$.
5. Determine the minimum gradient magnitude for cells near highly reacted cells, $|\nabla c|_{crit,2}$.
   a. Calculate the lengths $l_{2,adj}$ and $l_{2,diag}$.
   b. Assign the characteristic length l_2 from $l_{2,adj}$ or $l_{2,diag}$ depending on whether $F_{max,adj}(i,j)$ or $F_{max,diag}(i,j)$ is greater than F_{crit}.
   c. Insure that the result of the l_2 calculation is not less than the smallest spacing between cell (i,j) and its adjacent neighbors.
   d. Calculate the value of $|\nabla c|_{crit,2}(i,j)$.
6. Given $|\nabla c|_{crit,1}$, $|\nabla c|_{crit,2}$, and F_{max}, modify $|\nabla c|$, if necessary.
   a. If either $F_{max} < F_{crit}$ and $|\nabla c| > |\nabla c|_{crit,1}$ or $F_{max} \geq F_{crit}$ and $|\nabla c| \geq |\nabla c|_{crit,2}$, then $|\nabla c|$ remains unchanged.
   b. If $F_{max} < F_{crit}$ and $|\nabla c| \leq |\nabla c|_{crit,1}$, then $|\nabla c|$ is set equal to zero.
   c. If $F_{max} \geq F_{crit}$ and $|\nabla c| < |\nabla c|_{crit,2}$, then $|\nabla c|$ is set equal to $|\nabla c|_{crit,2}$.
7. Scale $|\nabla c|$ back to the local temperature.

Determination of model constants

The gradient model contains three numerical constants: C_1, C_2, and F_{crit}. To establish the sensitivity of the model to values of these constants, a test problem was formulated on a uniform 10 x 10 planar grid. The cell size is 1.0 cm square. All of the cells except for cell (1,1) contain a stoichiometric mixture of fuel and oxidant. Cell (1,1) contains the amount of product that would result from complete reaction of the initial mixture in any of the other cells. This simulates a reaction kernel in a totally premixed reactant field. Since there is no convection or other timestep

limiting process in this test, the numerical timestep may be chosen arbitrarily and, as such, is set to 1.0 s. The input burning velocity is chosen to be 0.01 cm/s, so that the time for the front to traverse a cell is long enough to provide adequate time resolution of the test results. In time, the reaction front expands and the radius of the front increases by one cell every 100 timesteps. A test problem with timestep 0.001 s and burning velocity 10 cm/s would produce identical results. Each of the tests was run for 1000 steps.

Before proceeding with the test problem, it is useful to define some terminology. In general, the reaction front can advance across a cell with any orientation with respect to the planar axes. Two specific orientations are at the focus of this study: horizontal and diagonal. A *horizontal cell* is one for which the reaction front advances horizontally across the cell. For the test problem this implies cells $(1,j)$, $j = 1,\ldots,10$. A *diagonal cell* is a cell in which the front crosses diagonally, i.e., cells (i,i), $i = 1,\ldots,10$. Note that by symmetry vertical cells are identical to the horizontal ones in this test problem.

Several different, specific timesteps in a calculation are also helpful in interpreting the results. That timestep during which a cell first reacts is denoted *fr* and that timestep when reaction is first completed in a cell is *cr*. Tables Ia and Ib contains *fr* and *cr* values from a test in which $C_1 = C_2 = 0.67$ and $F_{crit} = 0.95$. Note that a given cell can begin reacting before reaction is completed in its neighbors. Thus the reaction region will extend over several cells at a given time. The timestep *fr* is an indicator of the leading edge of the reaction region and *cr* in an indicator of the trailing edge. The difference between *fr* and *cr* for a given cell is the *cell reaction time*. (Since the numerical timestep is set at unity, the difference between *fr* and *cr* is not only the number of timesteps the calculation has proceeded but also the time elapsed.) The steady-state thickness of the reaction region is not well established until the horizontal and diagonal cell reaction times have reached a constant value along their respective directions of the front advancement. This typically does not occur until reaction is complete in all the cells diagonally adjacent to the reaction kernel. After the reaction region has been established, the cell reaction times are approximately equal to the ratio of the thickness of the reaction region and the input flame velocity. For the example in Tables Ia and Ib, the horizontal and diagonal cell reaction times are 148. Thus, the reaction zone is approximately 1.48 cells thick. This test is further discussed below.

Two final definitions are a measure of the burning velocity derived from the calculations. These quantities provide a test of consistency between input and output. The difference between *fr* (or *cr*) for one horizontal cell and *fr* (or *cr*) for its adjacent neighbor cell is the number of timesteps it takes the reaction front to advance through a horizontal cell. This quantity is called the *horizontal*

advance time. The counterpart for diagonal cells, the *diagonal advance time*, is the analagous difference between neighbors which are diagonal cells. For the present problem, a burning velocity of 0.01 cm/s and a cell length of 1.0 cm implies that the horizontal advance time should equal 100 and diagonal advance time should approximate $100 \times \sqrt{2}$ or 142.

The gradient model does not explicitly define the location of the reaction front, but we need such a definition to visualize the progress of a reaction. An appropriate tool for the present study is a contour plot of the *cr* values. The contours generated are called *reaction completion contours*, and the location of the front at any given timestep is defined as the reaction completion contour generated for that timestep. It should be emphasized that this definition of a front location is not necessary for use of the gradient model and it in no way affects the results of the model.

To begin the investigation of values for the constants, the value of F_{crit} was set to 0.95 and it was assumed that $C_1 = C_2 = C$. Typical reaction completion contours for a range of C values are shown in Figure 3. Tables of *fr* and *cr* such as those shown in Tables Ia and Ib were also generated. A summary of relevant information obtained from such tables for different values of C is shown in Table II.

The first question is how well do the various values of C reproduce the true horizontal and diagonal advance times. As hoped, the horizontal advance time is independent of C and the diagonal advance time is also little affected except for $C > 0.7$. Thus the input burning velocity is well reproduced over a large range of C values. We are free to select C based on more subtle reasons than simply having to reproduce the desired burning velocity. Table II shows that the horizontal cell reaction time is approximately equal to $1/(C \times V_b)$. This is true for all values of C. The diagonal cell reaction time also varies with $1/(C \times V_b)$, but the relationship is not as strong. The net result is that the curves of the horizontal and diagonal cell reaction times cross at approximately $C = 0.67$.

The equality of the horizontal and diagonal cell reaction times has two desirable properties. First, since the cell reaction time is proportional to the reaction region thickness, equality of the horizontal and diagonal times insures that the reaction region has a uniform thickness, irregardless of the orientation of the reaction region. Second, once the reaction region has become established, equality of the times insures the the reaction region will propagate with little additional distortion.

The contour plots in Figure 3 reinforce the choice of $C = 0.67$. Recall that for the test problem the reaction front should propagate as concentric circles after the initial square cell has smoothed out. Even though the horizontal and diagonal advance times equal their true values for $C < 0.8$, the contours are most accurately circular for C near 0.67. The cause of the flattening for $C < 0.67$ can be traced to the time needed to completely react the horizontal and diagonal cells directly connected

to the reaction kernel cell. The values of cr for cells (1,2) and (2,2) are also shown in Table II along with the difference between them. For the smaller values of C, the difference indicates that the front initially propagates much more quickly in the horizontal and vertical directions than along the diagonals. The result is the perceived flattening. Because the diagonal cell reaction times are less than their horizontal counterparts for these values of C, the reaction fronts would eventually appear more circular after an additional, significant delay.

The initial test cases assumed $C_1 = C_2$. The next set of tests, shown in Tables III and IV, assume $C_1 \neq C_2$. Again F_{crit} is set to 0.95. The most obvious result is that the horizontal advance time equals its true value only if C_1 and C_2 are equal. Thus, the initial assumption that $C_1 = C_2$ appears to be an optimal condition for the model.

Finally, the effects of varying F_{crit} were investigated, as shown in Table V. Here $C_1 = C_2 = 0.67$. The result is that $F_{crit} = 0.95$ appears to be optimum although distortions introduced by a slightly different value are minor. Varying C_1 and C_2 to improve the results for a different value of F_{crit} did not produce an optimum C value appreciably different from 0.67.

Selection of burning velocity

The burning velocity V_b is an input to this model. It may be specified as a constant value or may be a function of any relevant parameters. For example, V_b could be function of cell composition or temperature. The choice of burning velocity is totally independent of the front propagation model.

Change of species and energy release due to reaction

Given $|\nabla c|$, the change in species number density and the energy release can be calculated. The change in the number density of the product for a cell is

$$\Delta c = V_b \Delta t \, |\nabla c| \, . \tag{24}$$

It is important to insure that more product is not created than there are reactants available. The change in fuel number density is first calculated as the minimum of the amount of fuel needed to produce the change in number density of the product or the amount of fuel present. The same is true for the oxidant. Then

$$\Delta f = \min \left[\frac{N_f}{N_c} \Delta c, \; f \right] \tag{25a}$$

$$\Delta o = \min \left[\frac{N_o}{N_c} \Delta c, \; o \right] , \tag{25b}$$

where f and o are the fuel and oxidant number densities, respectively, N_f and N_o are the number of fuel and oxidant molecules consumed per reaction, and N_c is the number of product molecules produced per reaction. The actual species changes in number density are computed to assure consistency and mass conservation,

$$(\Delta f)' = \min\left[\Delta f,\ \frac{N_f}{N_o}\Delta o\right] \tag{26a}$$

$$(\Delta o)' = \min\left[\Delta o,\ \frac{N_o}{N_f}(\Delta f)'\right] \tag{26b}$$

$$(\Delta c)' = \min\left[\Delta c,\ \frac{N_c}{N_f}(\Delta f)',\ \frac{N_o}{N_f}(\Delta o)'\right]. \tag{26c}$$

The energy change is

$$\Delta e = \frac{(\Delta c)'}{N_c} \times \text{energy per reaction.} \tag{27}$$

This procedure guarantees mass conservation and appropriate energy release due to reaction.

Testing the Gradient Model

An extensive series of tests were performed to see if the gradient method reproduces the properties of a reaction front that propagates at a known velocity. This is a consistency test between input and output. For reacting but nonconvecting media, the reaction completion contours introduced above are used to track the progress of the front. For reactions occurring concurrently with convection, the reaction front is defined as the 0.80 contour of the $F_{i,j}$ values. All of the following tests were performed with $C_1 = C_2 = 0.67$ and $F_{crit} = 0.95$.

The first test was an extension of the test used to determine the model constants. Here a 20 x 20 uniform grid was initialized with a stoichiometric mixture of fuel and oxidant in all cells except for cell (10,10). Cell (10,10) contains the amount of product that would result from complete reaction in any of the other cells. There is no convection present in this test. The test was run for 1500 steps and the results are shown in Figures 4 and 5. The reaction completion contours in Figure 4 show that the reaction front propagates away from the reaction kernel in concentric circles and the spacing between the circles indicates that the front is propagating at the correct speed. The initial raggedness in the contours is due to the coarseness of the test grid. The innermost contour is diamond-shaped because the initial condition for the test consists of a step discontinuity at the interface, and the gradient method must propagate the interface through the cells adjacent to the initial reaction kernel before the interface profile can be established. The first contour for which the interface profile is established is the contour for step 200. It should be emphasized that the finite thickness of the profile is the numerical limit of resolution and is not a profile connected with the physical interface.

Figure 5 shows the time the front reaches a given distance from the reaction kernel. Time on the vertical axis is measured by cr and distance is measured from the center of the reaction kernel to the cell vertex farthest from the reaction kernel. This distance is chosen because reaction is not complete until the physical interface has reached this farthest point. The solid diagonal line in Figure 5 is the true position of an interface initiated at a point source located at the center of the actual reaction kernel and propagating with the speed V_b. The data points are the results of the test calculation. There are two reasons for the small displacement between the solid line and the data. First, the actual reaction kernel is not a point source and interface propagation begins on the square boundary of the reaction kernel. This explains the data point on the x-axis displaced from the origin, and that displacement is an upper estimate of the horizontal displacement of the other points. Adjustment for the finite reaction kernel moves the data points to the right. Second, there is a delay in the reaction completion of the cells adjacent to the reaction kernel. This delay is

related to the time it takes to establish the steady-state interface profile, and so all completion times are slightly longer than if the interface started with its steady-state propagation rate. Correction for this effect moves the data points down. The exact magnitude of each correction depends on the location of the point of interest with respect to the reaction kernel. If all points are corrected by the displacement of the data on the x-axis and the time delay for reaction completion of the cells horizontally adjacent to the reaction kernel cell, then the data points fall almost exactly on the point source solution line. These finite resolution corrections do not alter the slope of a line suggested by the data points in Figure 5, and this slope is almost identical to the input propagation speed.

The second test investigated the ability of the gradient model to handle merging fronts. A 40 x 40 uniform grid was used and two reaction kernels were specified. The test was run for 2100 steps. Figure 6 shows that the fronts merge without difficulty. The reaction fronts propagate independently until they merge, and then the merged front continues to propagate as the union of two independent fronts. The cusps seen at the points where the fronts merge occur because a constant propagation speed was specifed and no attempt was made here to model the finer details of the reaction. Several combinations of point and line reaction kernels have been tested in both flowing and stationary backgrounds, and the gradient model always handles interface merging well.

The next test case exercised the gradient model on a nonuniform grid. The grid is uniformly stretched left-to-right (x-direction) by a factor of 1.03 and uniformly stretched bottom-to-top (y-direction) by a factor of 1.07. The crosshatched rectangles in the corners of Figure 7 show the cell sizes and shapes at those locations. For this test, a single-cell reaction kernel was initialized in a premixed reactant field. The test was run for 2400 steps. Reaction completion contours are shown in Figure 7. The distortion in the three innermost contours occurs because the interface profile is not yet established. Any remaining deviations from a circular trace relax as the calculation proceeds. A graph of time as a function of distance from the reaction kernel is very similar to Figure 5, and again the slope suggested by the data is nearly identical to the specified propagation speed.

The remaining tests were performed in convecting flows. Since the gradient model keys on sharp gradients in the flow, it is important that the convection algorithm is not highly diffusive at the front, and any "wiggles" that distort the local gradient should not appear in the solution of the indicator variable. Here the Flux-Corrected Transport (FCT) algorithm [11] is used to transport mass, momentum, energy, and species in fast flows, and BIC-FCT [12], an implicit corrector used with the FCT algorithm, is used to convect slower flows. The expansion due to energy release

follows naturally from a source term in the energy conservation equation and does not require the calculation of a separate velocity field as is done, for example, in Ref. 13. Examples using both FCT algorithms will now be presented.

The first test with convection was performed on a uniform grid with an x-component velocity of 5 m/s and a y-component velocity of 10 m/s. A 3×3 reaction kernel was initialized in a premixed reactant field. The burning velocity was specified as 10 m/s. The standard FCT algorithm was used to simulate convection. A series of $F_{i,j} = 0.80$ contours are shown in Figure 8. The innermost contour represents the reaction front at timestep 100 and each successive contour shows the reaction front 100 timesteps later. All sides of the reaction front move with speeds which are the vector sum of the background velocity and the propagation speed in the direction of the outward normal. This results in the lower edge of the interface remaining stationary because the downward propagation just balances the flow. Note also that the initially square reaction front is becoming progressively more circular. Tests with convection and several merging interfaces show the same front behavior.

All of the previous tests were done without energy release. The final convection test involves a comparison of the evolution of the flow caused by a single vortex in a box when there is no reaction, when the reaction is isothermal, and when there is reaction with energy release. The flow is initialized with the velocities in the central "box" of a 3 x 3 array of potential point vortices. By locating the center of the central vortex at the intersection of computational grid lines, the calculation of velocities at the cell centers avoids the singularity at the vortex core. The circulation of each vortex is 10000 cm^2/s. A 40 cm square computational domain is used and the grid is slightly stretched to concentrate cells in the center of the box. The burning velocity is 200 cm/s and the timestep is 3.75×10^{-5} s. The upper half plane of the box is initialized with a stoichiometric mixture of fuel and oxidant and the lower half plane contains only product. The temperature of the entire field is 1000°K, except for the energy release case where the temperature of the products is 1950°K. The pressure is uniform at 1 atm. BIC-FCT was used for convection.

Figure 9 shows contours of $F_{i,j}$ at intervals of 0.1. For the nonreacting case, the vortex grows with time, but the detail of the vortex center is smeared due to numerical diffusion. This smearing is the result of the coarseness of the test grid. Otherwise, the velocity near the vortex center is sufficiently high to produce several windings of the central spiral. However, even with the numerical smearing, the interface is still symmetrically located about the vortex center. In the isothermal reaction case, several differences are seen. First, the propagation model tends to sharpen the interface. The distance between the 0.1 and 0.9 contours at the edges of the box has decreased because the propagation algorithm has reacted numerically diffused material. This

effect is most obvious near the vortex center where the reaction front is progressing into the vortex because the rate of reaction is exceeding the rate of numerical diffusion. The contours are not symmetric because 1) the reaction model is only active on the product side of the interface and so interface sharpening cannot occur on the reactants side, and 2) the reaction front is propagating into the reactants arm of the vortex spiral. Because there is no energy release in the isothermal case, the mass, momentum, and energy is unchanged from the nonreacting case. Only the individual species concentrations are altered by the reaction. This is not the situation when the material conversion is accompanied by energy release. In that case the vortex flow is augmented due to the expansion, and this causes the reactants not only to be consumed due to reaction but also pushed away from the neighborhood of the vortex center into lower velocity parts of the box. The interface sharpening effect is still present. Together, the continued presence of the interface sharpening and the expansion in a direction away from the reaction location indicate that the energy deposition is being done correctly. In all convecting cases, the interface moves with the sum of the flow and propagation velocities.

Discussion

The gradient method has been developed to propagate an interface which is characterized by large gradients due to conversion of material at the interface. Although the development and testing described above were done for two-dimensional problems, the formulation can easily be extended to three dimensions. Unlike other interface tracking methods, the gradient method does not require the location and movement of the interface to be defined explicitly. Only the effects of the interface are considered. The gradient method has demonstrated its ability to simulate reaction at an interface on uniform or stretched grids. There is no limit to the number of interfaces which can be present and any number of merging interfaces can be handled without difficulty.

This version of the gradient method uses the product number density as the indicator variable, but other versions are possible using other indicators. For example, assuming that expansion due to energy release causes proportionate amounts of the species in a cell to leave that cell indicates that using the product volume fraction as the indicator would eliminate the need of scaling to a reference temperature. However, this choice may not reduce the total number of arithmetic operations used. The approach presented in this paper is sufficiently general to accommodate a variety of alternate indicator variables.

As well as the gradient method has been shown to perform, there are still some limitations, many of which also apply to the volume tracking methods. Because the location of the interface is known only approximately, information such as the curvature of the interface must be derived from a separate calculation. For example, Ghoniem [14] has recently used an approach similar to Chorin's idea of osculating circles [15] to estimate the curvature of a reaction front defined by SLIC [4,16]. A more important limitation of any method that reconstructs the interface on the basis of a marker or indicator quantity is that care must be taken to insure that the presence of the indicator in a cell is solely the result of reaction in that cell. For example, small amounts of the indicator numerically diffused from the reaction front should not result in the identification of spurious interfaces. This care is necessary regardless of the choice of marker or indicator variable.

The concern over the extraneous appearance of the indicator away from the interface highlights the need to choose a convection algorithm which avoids excessive numerical diffusion. Additionally, the convection algorithm should be monotonic so that no wiggles appear in the indicator profile which will introduce large errors in the estimation of the gradient. The present implementation has tested two variations of the FCT algorithm to satisfy this requirement.

Finally, an important requirement for any algorithm that is to be used in a numerical simulation is that it allows full use of vector and parallel computing systems. The program logic of the new

method vectorizes fully. In addition, if the chosen indicator variable is already included in the calculation, then no extra array storage is necessary beyond whatever scratch space is useful to enhance vectorization.

Acknowledgements

This work was supported by the Office of Naval Research and the Naval Research Laboratory. We especially thank Professor Norman Chigier for encouraging this work. Also, we would like to thank Dr. Gopal Patnaik whose insightful questions helped to clarify many ideas.

References

1. J. Glimm, O. McBryan, R.Menikoff, and D. Sharp, *SIAM J. Sci. Stat. Computing* **7** (1986), 230.
2. I-L. Chern, J. Glimm, O. McBryan, B. Plohr, and S. Yaniv, *J. Comput. Phys.* **62** (1986), 83.
3. A.A. Amsden, "The Particle-in-Cell Method for the Calculation of the Dynamics of Compressible Fluids," Los Alamos Scientific Laboratory, LA-3466, 1966.
4. W.F. Noh and P. Woodward, "SLIC (Simple Line Interface Method)," *Proceedings of the Fifth International Conference on Numerical Methods in Fluid Dynamics*, in *Lecture Notes in Physics* (A.I. van de Vooren and P.J. Zandbergen, eds.), vol. 59, (Springer-Verlag, New York, 1976), p.330.
5. C.W. Hirt and B.D. Nichols, *J. Comput. Phys.* **39** (1981), 201.
6. M.J. Fritts and J.P. Boris, *J. Comput. Phys.* **31** (1979), 173.
7. A. Harten and J.M. Hyman, *J. Comput. Phys.* **50** (1983), 235.
8. W.F. Noh, "CEL: A Time-Dependent, Two-Space-Dimensional, Coupled Eulerian-Lagrange Code," *Methods in Computational Physics* (B. Adler, S. Fernbach, and M. Rothberg, eds.), vol. 3, (Academic Press, New York, 1964), p. 117.
9. J.M. Hyman, *Physica* **12D** (1984), 396.
10. K.J. Laskey, E.S. Oran, and J.P. Boris, "Approaches to Resolving and Tracking Interfaces and Discontinuities," Naval Research Laboratory, NRL Memorandum Report 5999, 1987.
11. J.P. Boris, and D.L. Book, "Solution of Continuity Equations by the Method of Flux-Corrected Transport," *Methods in Computational Physics* (B. Adler, S. Fernbach, and M. Rothberg, eds.), vol. 16, (Academic Press, New York, 1976), p. 85.
12. G. Patnaik, R.H. Guirguis, J.P. Boris, and E.S. Oran, "A Barely Implicit Correction For Flux-Corrected Transport," to appear in *J. Comput. Phys.* (1987).
13. A.F. Ghoniem, A.J. Chorin, and A.K. Oppenheim, *Phil. Tran. T. Soc. Lond.* **A304** (1982), 303.
14. A.F. Ghoniem and O.M. Knio, "Numerical Simulation of Flame Propagation in Constant Volume Chambers," presented at *Twenty-First Symposium (International) on Combustion*, Munich, Germany, August 3-8, 1987.
15. A.J. Chorin, *J. Comput. Phys.* **58** (1985), 472.
16. A.J. Chorin, *J. Comput. Phys.* **35** (1980), 1.

Table Ia. *Timestep of first reaction, fr.*

J\I	1	2	3	4	5	6	7	8	9	10
1	0	1	92	190	289	389	488	588	688	788
2	1	1	119	212	308	405	502	600	699	798
3	92	119	150	250	345	437	531	626	722	819
4	190	212	250	305	387	481	571	663	756	850
5	289	308	345	387	452	528	618	707	797	888
6	389	405	437	481	528	596	670	755	844	933
7	488	502	531	571	618	670	738	812	894	982
8	588	600	626	663	707	755	812	881	954	***
9	688	699	722	756	797	844	894	954	***	***
10	788	798	819	850	888	933	982	***	***	***

Table Ib. *Timestep when reaction is completed, cr.*

J\I	1	2	3	4	5	6	7	8	9	10
1	0	137	237	337	436	536	636	736	836	936
2	137	154	255	353	451	549	647	746	845	946
3	237	255	309	393	486	580	675	771	867	966
4	337	353	393	458	534	623	714	807	900	997
5	436	451	486	534	601	675	761	851	941	***
6	536	549	580	623	675	744	818	900	988	***
7	636	647	675	714	761	818	886	960	***	***
8	736	746	771	807	851	900	969	***	***	***
9	836	845	867	900	941	988	***	***	***	***
10	936	946	966	997	***	***	***	***	***	***

Table II. *Derived values for $C_1 = C_2 = C$ and $F_{crit} = 0.95$.*

C	horizontal advance time	diagonal advance time	horizontal cell reaction time	diagonal cell reaction time	cr (1,2)	cr (2,2)	$cr(2,2) - cr(1,2)$
0.40	100	143	248	222	153	215	62
0.50	100	143	199	185	149	190	41
0.60	100	142	166	153	144	166	22
0.67	100	142	148	148	137	154	17
0.70	100	142	141	147	133	150	17
0.80	100	132	124	138	122	138	16
0.90	100	122	111	127	111	131	20
1.00	96	111	100	115	101	123	22

Table III. *Derived values for* C_1 *variable,* $C_2 = 0.67$, *and* $F_{crit} = 0.95$.

C_1	horizontal advance time	diagonal advance time	horizontal cell reaction time	diagonal cell reaction time	cr (1,2)	cr (2,2)	$cr(2,2)-cr(1,2)$
0.50	88	133	161	163	140	165	25
0.60	94	142	152	153	140	158	18
0.67	100	142	148	148	137	154	17
0.70	104	143	144	148	135	153	18
0.80	111	143	135	148	131	152	21

Table IV. *Derived values for* $C_1 = 0.67$, C_2 *variable, and* $F_{crit} = 0.95$.

C_2	horizontal advance time	diagonal advance time	horizontal cell reaction time	diagonal cell reaction time	cr (1,2)	cr (2,2)	$cr(2,2)-cr(1,2)$
0.50	107	142	156	148	136	178	42
0.60	105	143	153	148	139	162	23
0.67	100	142	148	148	137	154	17
0.70	97	141	143	147	135	151	16
0.80	89	130	129	136	123	141	18

Table V. *Derived values for* $C_1 = C_2 = 0.67$ *and* $F_{crit} = F$.

F	horizontal advance time	diagonal advance time	horizontal cell reaction time	diagonal cell reaction time	cr (1,2)	cr (2,2)	$cr(2,2)-cr(1,2)$
0.80	100	132	148	160	137	157	20
0.90	100	141	148	154	137	154	17
0.95	100	142	148	148	137	154	17
0.99	100	142	148	143	137	154	17

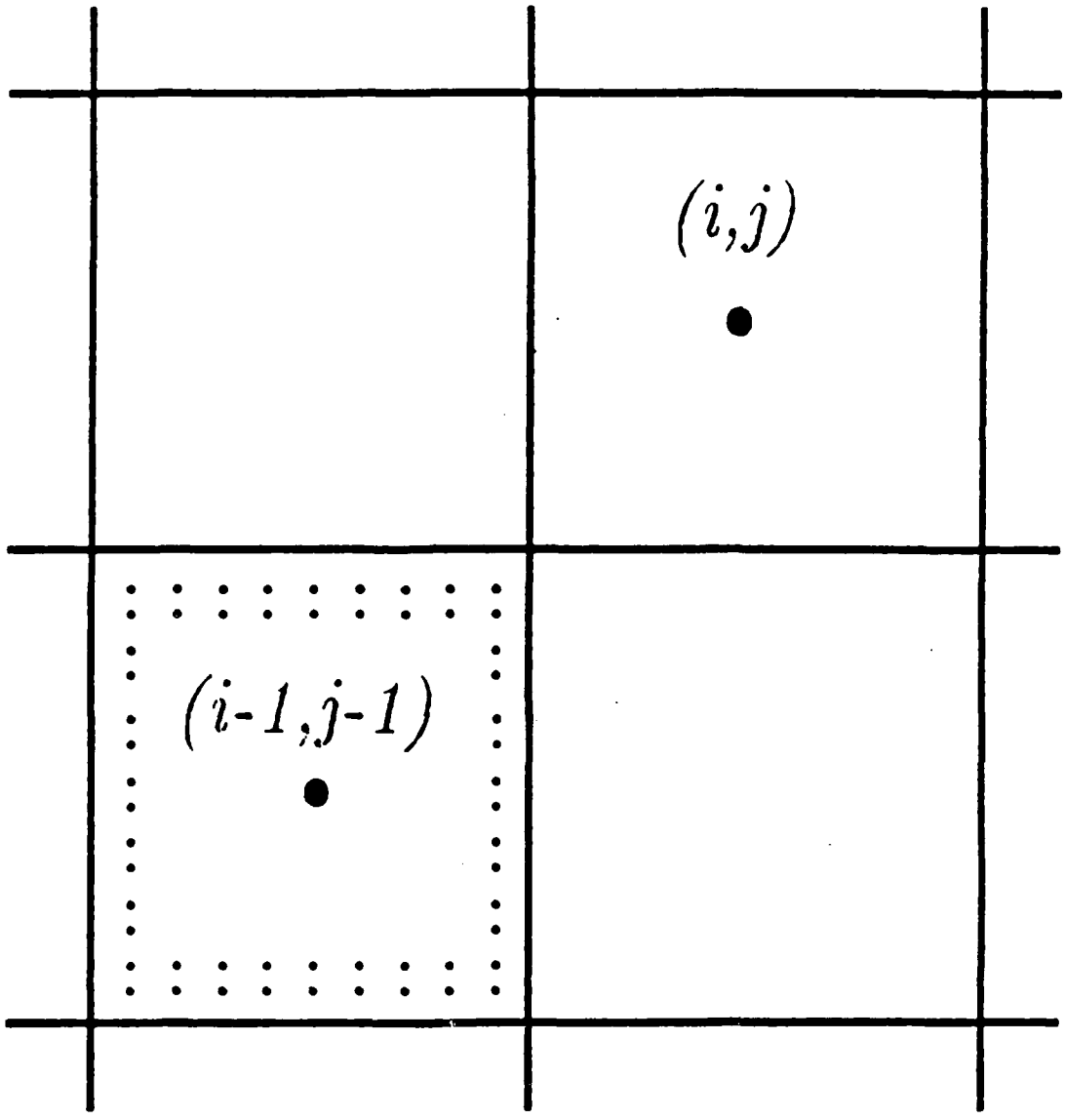

Figure 1. *Cell (i, j) has a highly reacted diagonal neighbor, (i-1, j-1).*

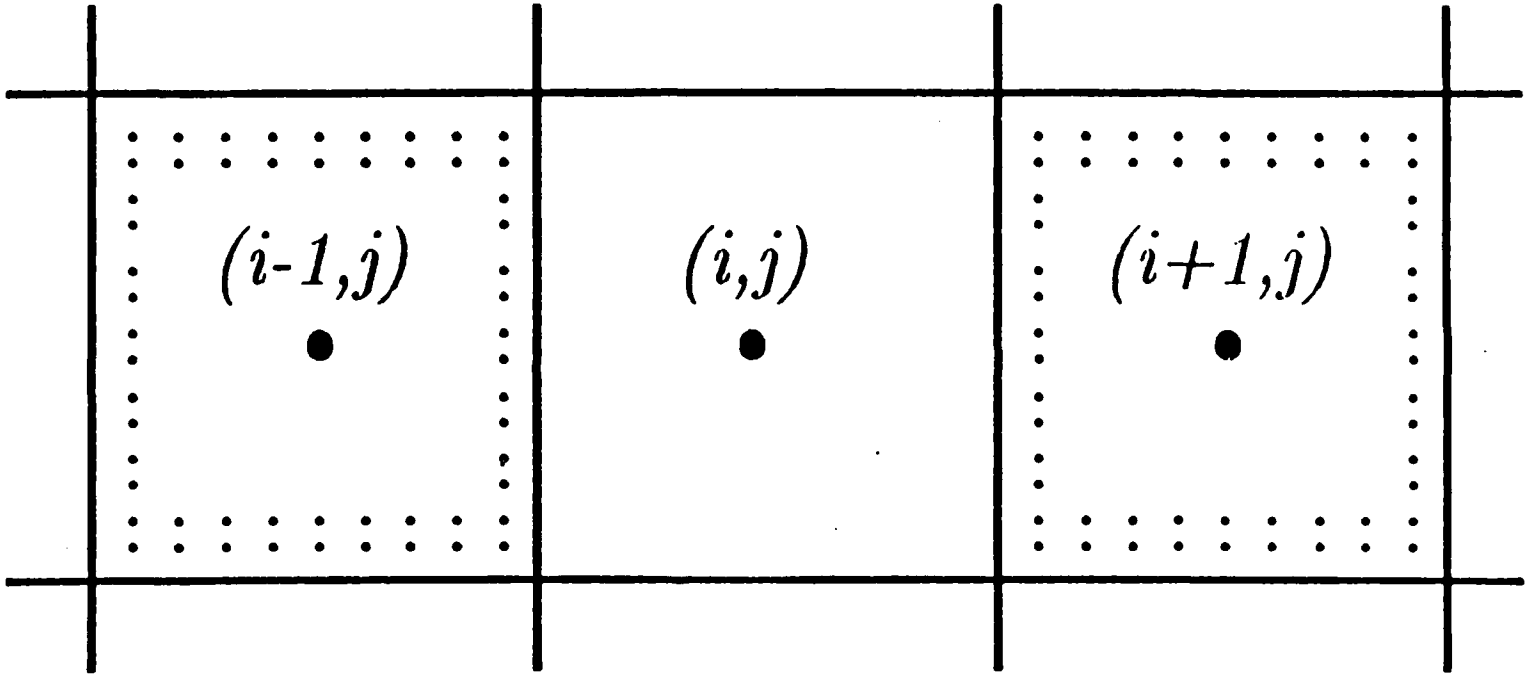

Figure 2. *Cell(i, j) is between two merging interfaces.*

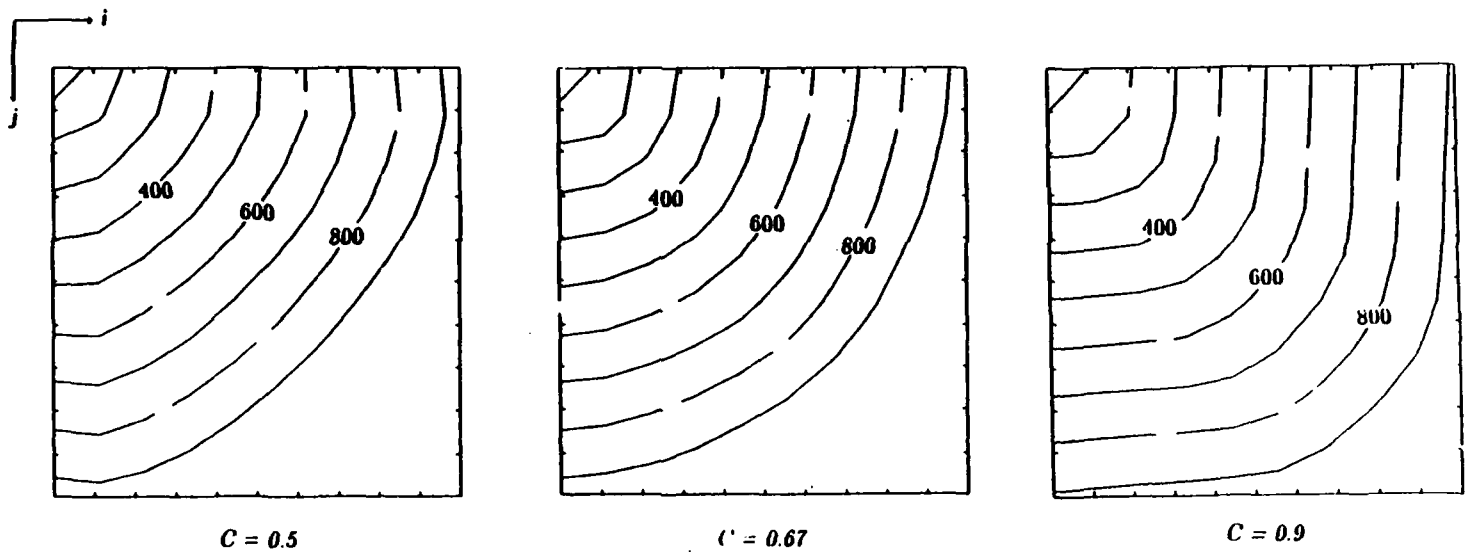

Figure 3. *Reaction completion contours at step 1000.*

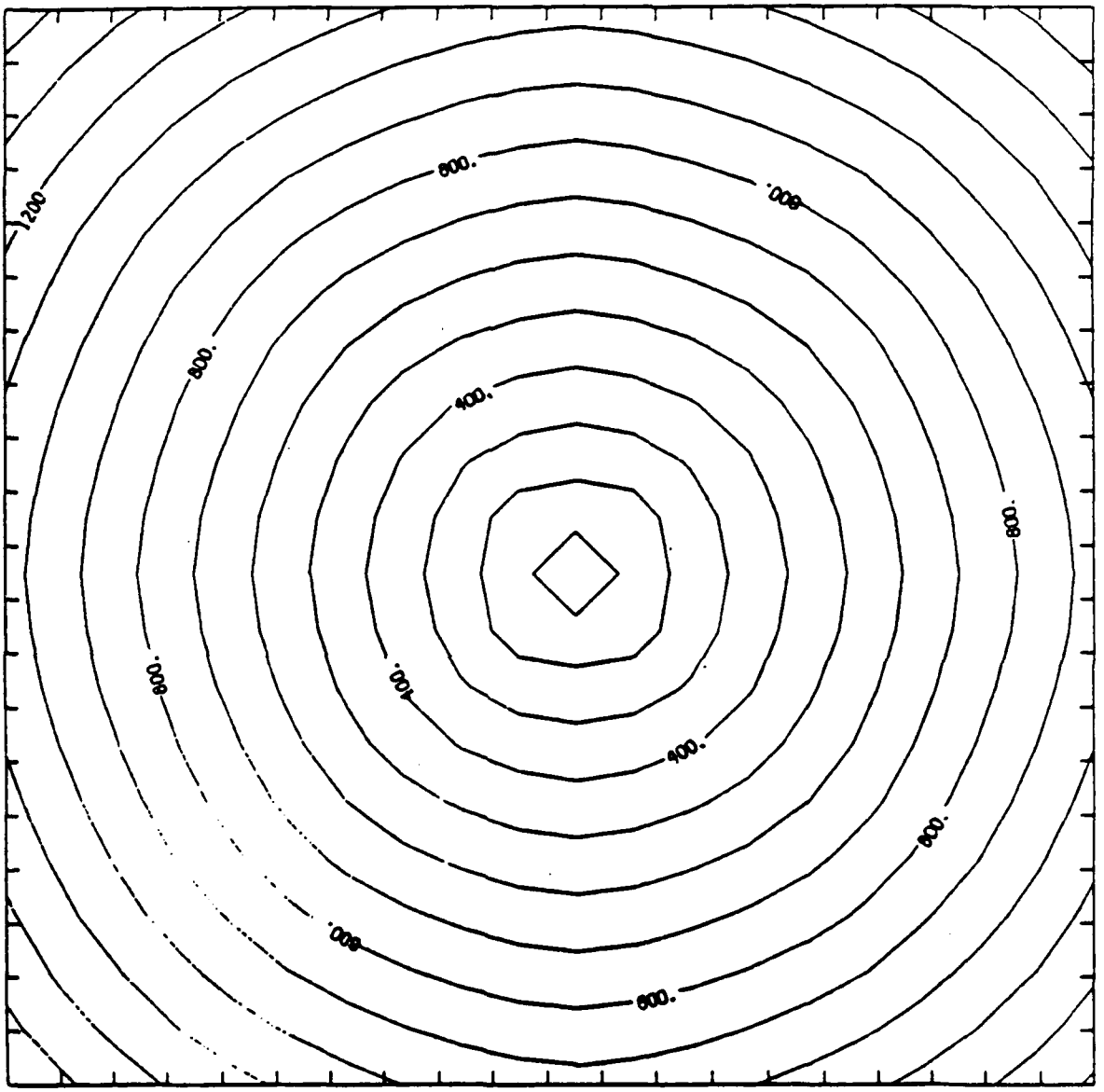

Figure 4. *Reaction completion contours for Test 1.*

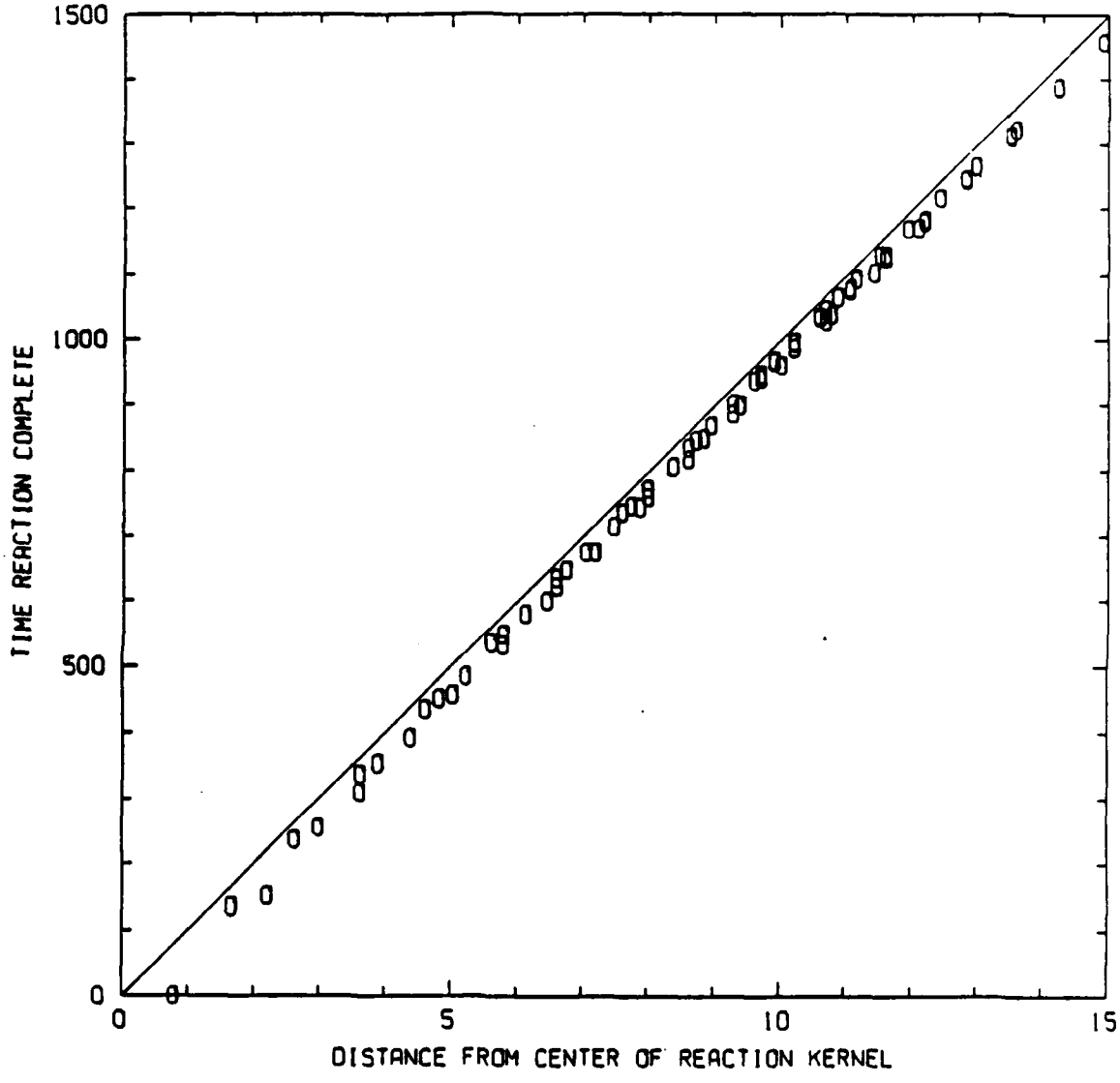

Figure 5. *Propagation distance vs. time for Test 1 (uncorrected data).*

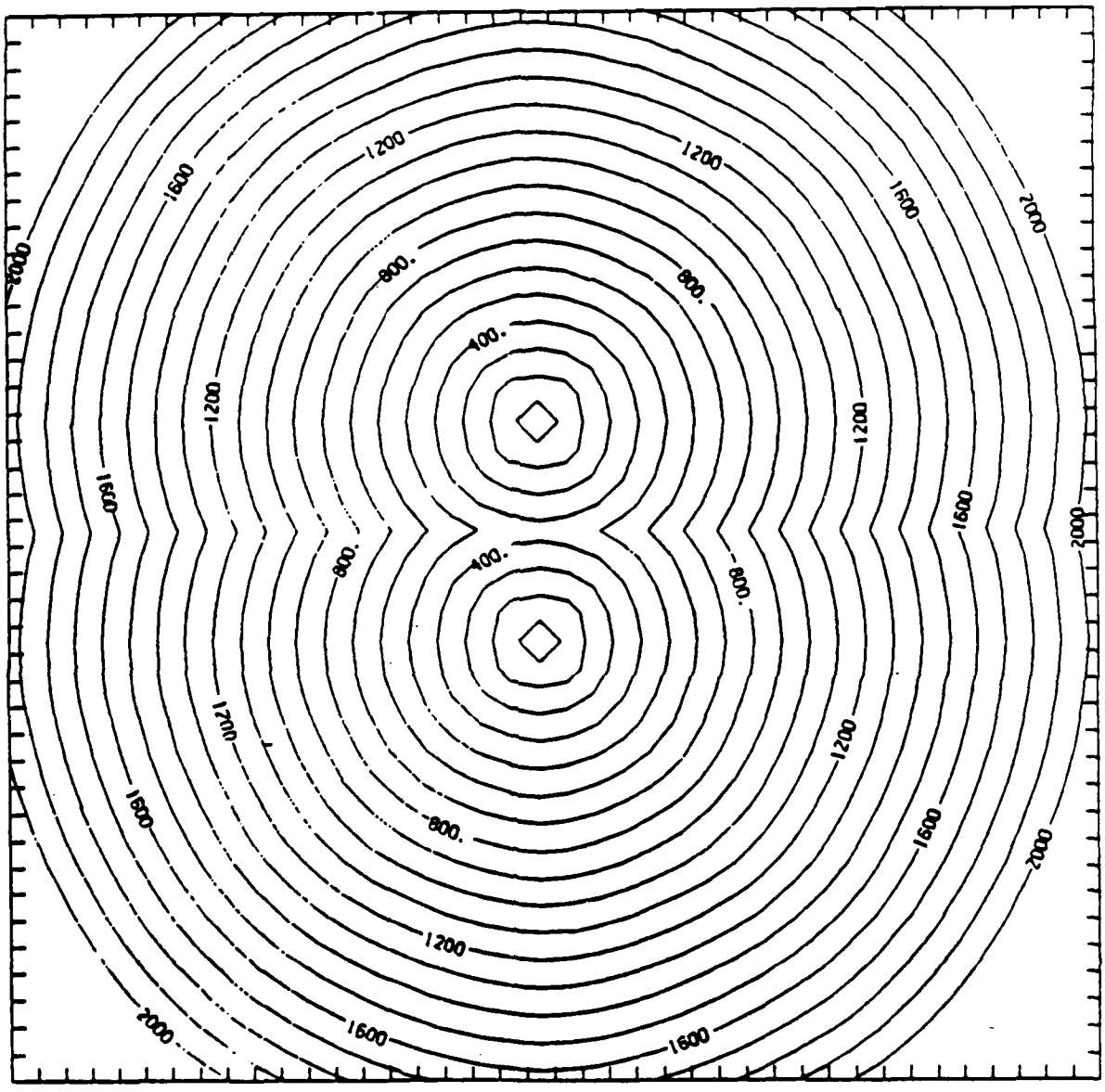

Figure 6. *Reaction completion contours for merging interfaces.*

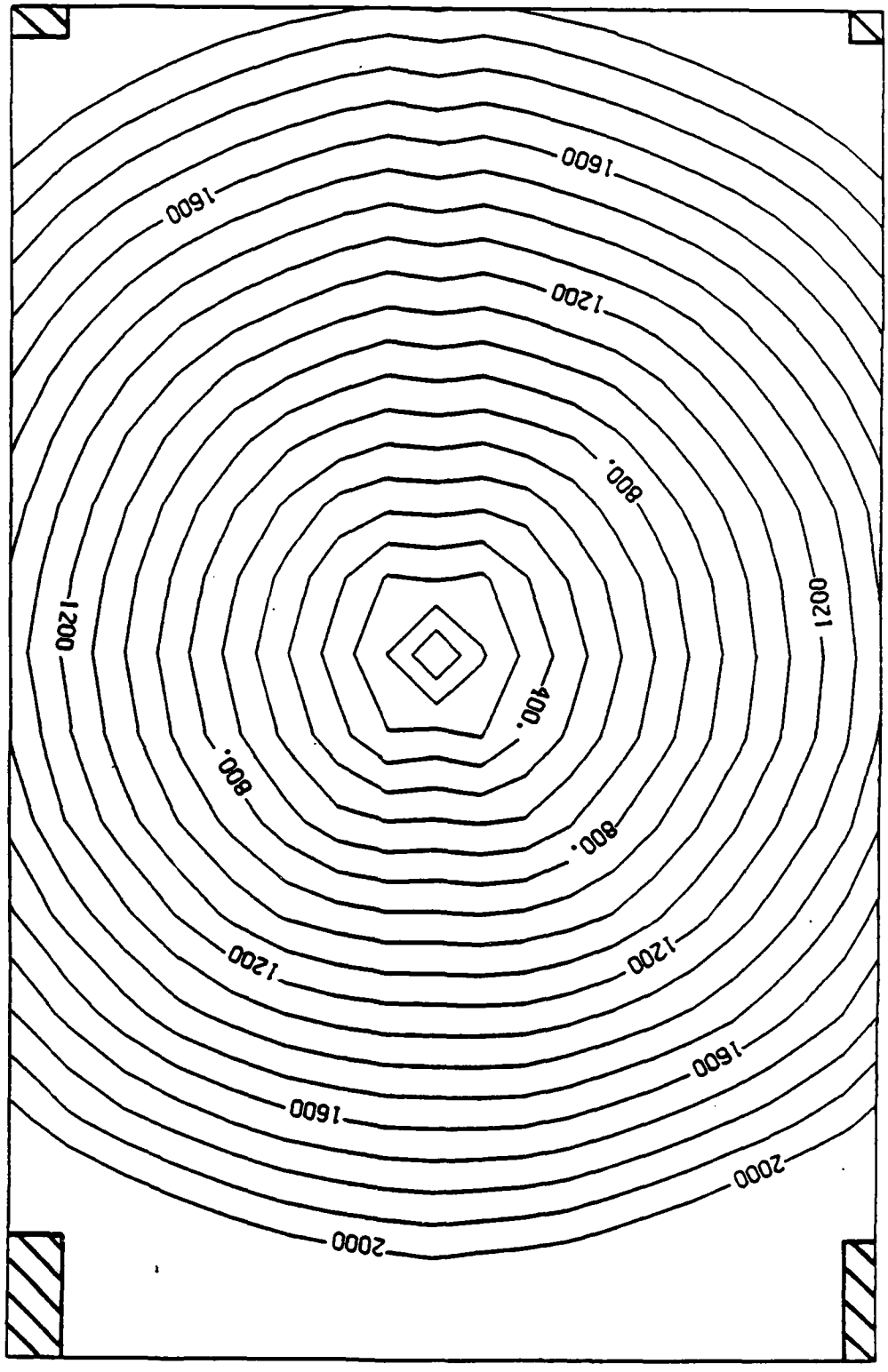

Figure 7. *Reaction completion contours for Test 3.*

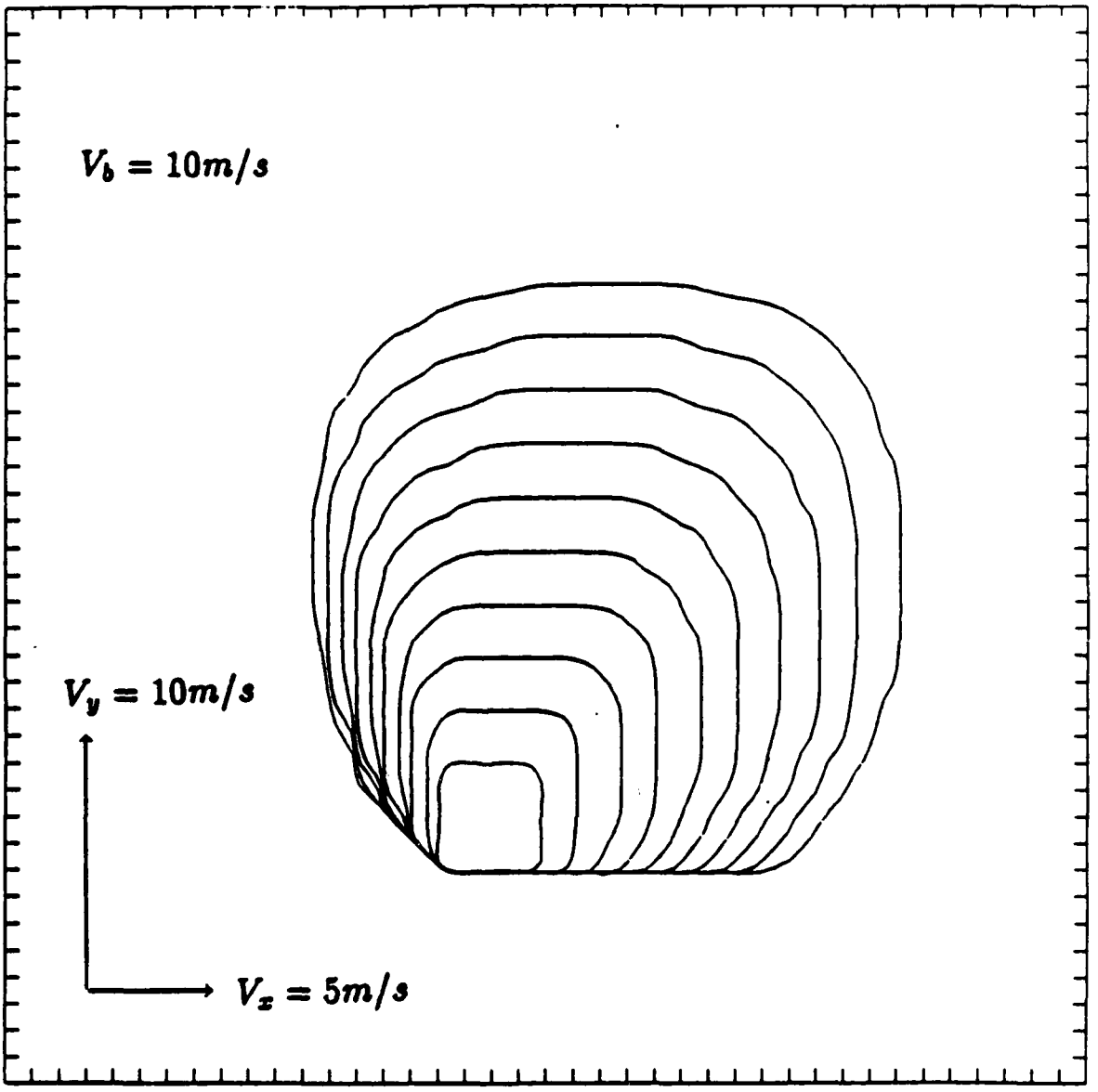

Figure 8. $F_{i,j} = 0.80$ *contours for convection test.*

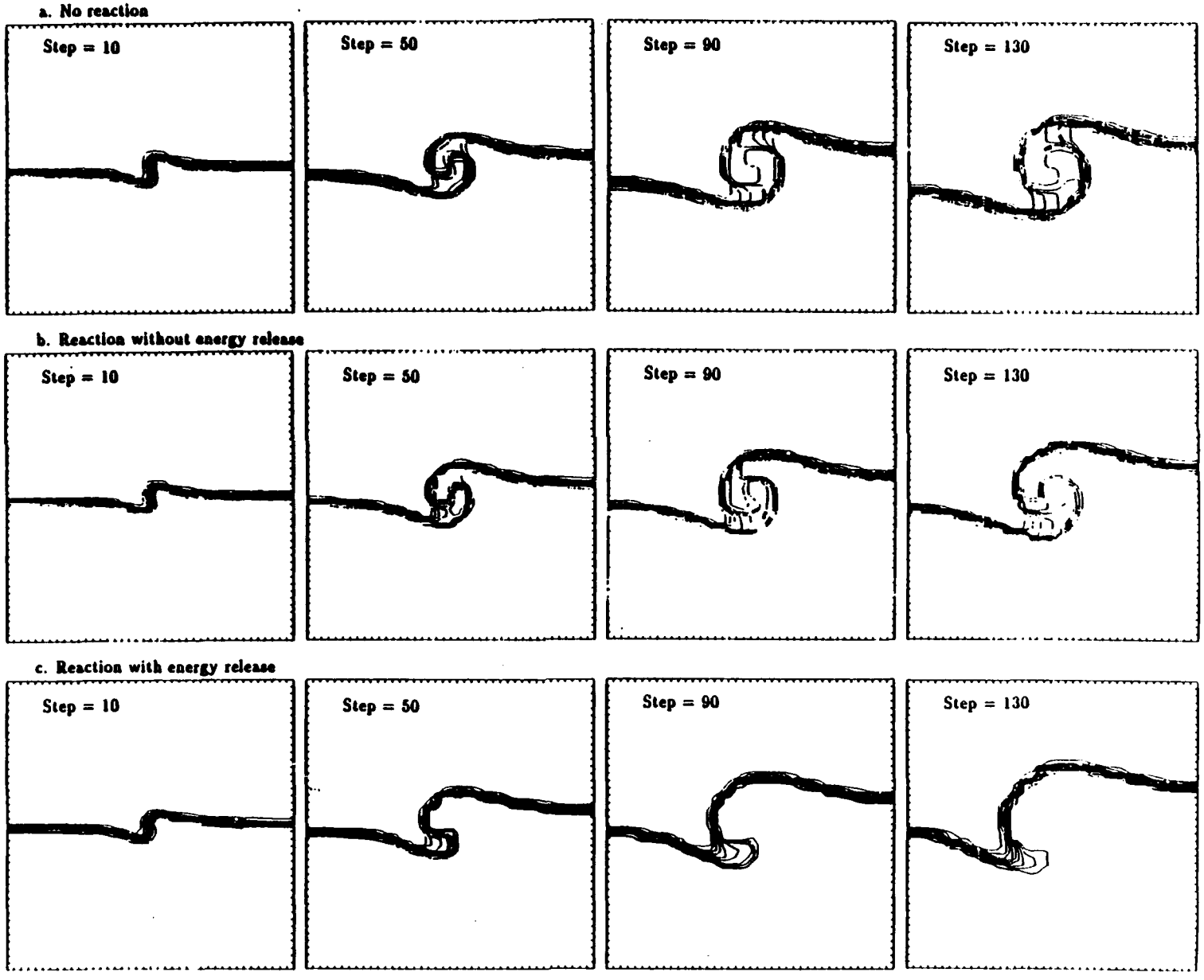

Figure 9. $F_{i,j}$ *contours for vortex tests. (Topmost contour,* $F_{i,j} = 0.1$*; bottommost contour,* $F_{i,j} = 0.9$*.)*

END
DATED
FILM
8-88
DTIC